Available online at www.sciencedirect.com
ScienceDirect
Trans. Nonferrous Met. Soc. China 24(2014) 2870−2876
Transactions of Nonferrous Metals Society of China
www.tnmsc.cn

Effect of bias voltage on microstructure and nanomechanical properties of Ti films

Ying-long LIU[1], Fang LIU[2], Qian WU[2], Ai-ying CHEN[2], Xiang LI[2], Deng PAN[2]

1. School of Mechanical Engineering, University of Shanghai for Science and Technology, Shanghai 200093, China;
2. School of Materials Science and Engineering, University of Shanghai for Science and Technology, Shanghai 200093, China

Received 26 September 2013; accepted 3 December 2013

Abstract: In order to investigate nanomechanical properties of nanostructured Ti metallic material, pure Ti films were prepared by magnetron sputtering at the bias voltage of 0−140 V. The microstructure of Ti films was characterized by X-ray diffraction (XRD), scanning electron microscopy (SEM) and high-resolution transmission electron microscopy (HRTEM). It is interesting to find that the microstructure of pure Ti films was characterized by the composite structure of amorphous-like matrix embodied with nanocrystallines, and the crystallization was improved with the increase of bias voltage. The hardness of Ti films measured by nanoindentation tests shows a linear relationship with grain sizes in the scale of 6−15 nm. However, the pure Ti films exhibit a soft tendency characterized by a smaller slope of Hall−Petch relationship. In addition, the effect of bias voltage on the growth orientation of Ti films was discussed.

Key words: Ti film; magnetron sputtering; bias voltage; nanocrystalline; Hall−Petch relationship

1 Introduction

Nowadays, Ti films are widely used in aerospace engineering, medical instrument and construction industry because of the superior properties, such as excellent thermal stability and good corrosion resistance [1−3]. Magnetron sputtering, which is a well-established physical vapor deposition technique, has been widely applied to preparing dense and uniform metallic thin films [4−7]. The effect of sputtering process on the microstructure of Ti films has been studied, such as substrate temperature [4,8], sputtering power [6,9], discharge pressure and bias voltage [10,11]. Among these parameters, the bias voltage seriously influences the microstructures of thin films, such as surface topography, preferred orientation [11,12], deposition rate [11] and film density [13]. Recently, ZHANG et al [12] reported that increasing the substrate bias voltage caused an increment of lattice constant and a transition of preferred orientation from (002) to (100) planes of He−Ti films induced by the implantation of He. The orientation transition of Ti film trigged by negative bias voltage was also reported in Ref. [11], which showed the diffraction peaks of Ti films changed from (111) to (200) planes with negative bias voltage increasing from 15 to 260 V. However, the detailed microstructure and effect of microstructure transition on nanomechanical properties were less reported. In the present work, the bias voltage in the range of 0−140 V was applied to depositing Ti films by magnetron sputtering. A composite structure of amorphous-like matrix embodied with nanocrystallines was observed, and the effect of bias voltage on the crystallization was discussed. The nanoindentation tests were carried out to explore the Hall−Petch relationship extending grain size to several nanometers scales.

2 Experimental

Ti films were deposited on (100) monocrystal silicon by direct current magnetron sputtering at room temperature. A pure titanium target (99.995%) with diameter of 50.8 mm and thickness of 5 mm was used.

Foundation item: Projects (51102264, 51271123) supported by the National Natural Science Foundation of China; Projects (5313310202, 13ZR1427900) supported by Shanghai Municipal Education Commission, China
Corresponding author: Ai-ying CHEN; Tel: +86-21-55271708; Fax: +86-21-55270632; E-mail: aychen@usst.edu.cn
DOI: 10.1016/S1003-6326(14)63420-8

The Si substrates were cleaned with acetone, ethyl alcohol and deionized water in ultrasonic bath for 20 min, respectively, before they were fixed in a vacuum chamber. Bias voltage was applied by 0, 60, 100 and 140 V, respectively. The other detailed parameters are listed in Table 1. Before the experiment was started, the target was pre-sputtered for 10 min.

Table 1 Deposition parameters of Ti films on Si (100) substrates by magnetron sputtering

Background pressure/ Pa	Ar flow/ (mL·min^{-1})	Work pressure/ Pa	Work power/ W	Target-substrate distance/mm	Sputtering time/ min
1.5×10^{-5}	20	0.5	200	80	20

A Bruker D8 X-ray diffractometer (XRD) with Cu K_α radiation was used to identify the phase structure. The XRD tests were carried out with a scan rate of 0.02 s/step and in a scan range of 30°−70°. The surface topography was observed by FEI Quanta 450 emission scanning electron microscope (SEM) at the acceleration voltage of 20 kV. The Tecnai G2 F30 transmission electron microscope (TEM) was used under an operating voltage of 200 kV. The plane-view TEM foils were ion-thinned at low temperature. The hardness was measured by nano indenter (Agilent G200) using the continuous stiffness measurement technique [14]. The normal force of the indenter (a Berkovich diamond tip) was applied to the sample surface increasing from 0 to 1 mN with the loading speed of 5 nm/s and the track length was about 80 nm. The statistical mean hardness was evaluated from at least 25 indentations. The atomic force microscopy (AFM, Shimadzu N9500) was used to determine the surface roughness under a semi-contact (tapping) mode with the scan area of 5 μm× 5 μm. The surface roughness was expressed by root mean square roughness.

3 Results

3.1 Orientation analysis

The XRD patterns of Ti films deposited at different bias voltages are shown in Fig. 1. The pure Ti films are produced in all samples identified by the diffraction peaks. However, the crystal orientation is changed. The (002) diffraction peak is the only strongest peak in the Ti film deposited at 0 V, indicating the obviously (002) preferred growth. However, when the bias voltage increases, the polycrystal orientation occurs, and (100) and (101) planes present the highest intensity at the bias voltage of 100 V. Nevertheless, (002) orientation enhances again at the bias voltage of 140 V. The XRD results show a transition from (002) preferred orientation to random polycrystalline structure under applied bias voltages.

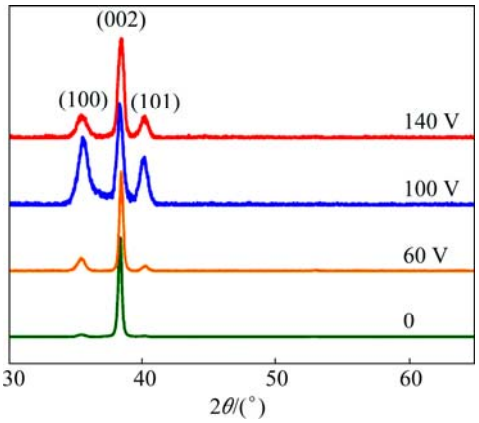

Fig.1 XRD patterns of Ti films deposited at different bias voltages

3.2 Surface morphology

The surface topography of Ti films deposited at different bias voltages is shown in Fig. 2. The clusters with three-dimensional structure (marked by arrows) are observed at the bias voltage of 0 and 60 V, especially the Ti film prepared at 60 V, as shown in Figs. 2(a) and (b). The root mean square roughnesses of the Ti films deposited at 0 and 60 V are 10 and 12 nm, respectively. When the bias voltage increases to 100 V, the three-dimensional clusters disappear, and the surface becomes uniform, dense and flat, showing the smallest surface roughness (7 nm) among all Ti films, as shown in Fig. 2(c). When the bias voltage is 140 V, a relative flat surface is obtained compared with the Ti films sputtered at 0 and 60 V, as shown in Fig. 2(d).

The cross-sectional SEM images exhibit that the Ti films grow in a columnar structure perpendicular to the Si substrate, as shown in Fig. 3. The diameter of the columnar clusters is the lowest for the Ti film deposited at the bias voltage of 0 V (Fig. 3(a)). The compact density of Ti film deposited at 0 or 100 V is better, as shown in Figs. 3(a) and (c), respectively. While voids occur at the center of the Ti films deposited at 60 and 140 V, respectively, as indicated by arrows in Figs. 3(b) and (d). Coarsening is observed at the cross section of the Ti film sputtered at 140 V, where columnar clusters are finer at the bottom and grow up with the increase of film thickness, as separated by line in Fig. 3(d). The thickness of Ti films is decreased with the increase of bias voltage, as marked in Fig. 3, which means the reduced deposition rate. The average deposition rate is estimated according to the measured thickness divided by sputtering time, as shown in Fig. 4. The deposition rate exhibits a nonlinear decrease with the increase of bias voltage, which may be originated from the occurrence of re-sputtering [15].

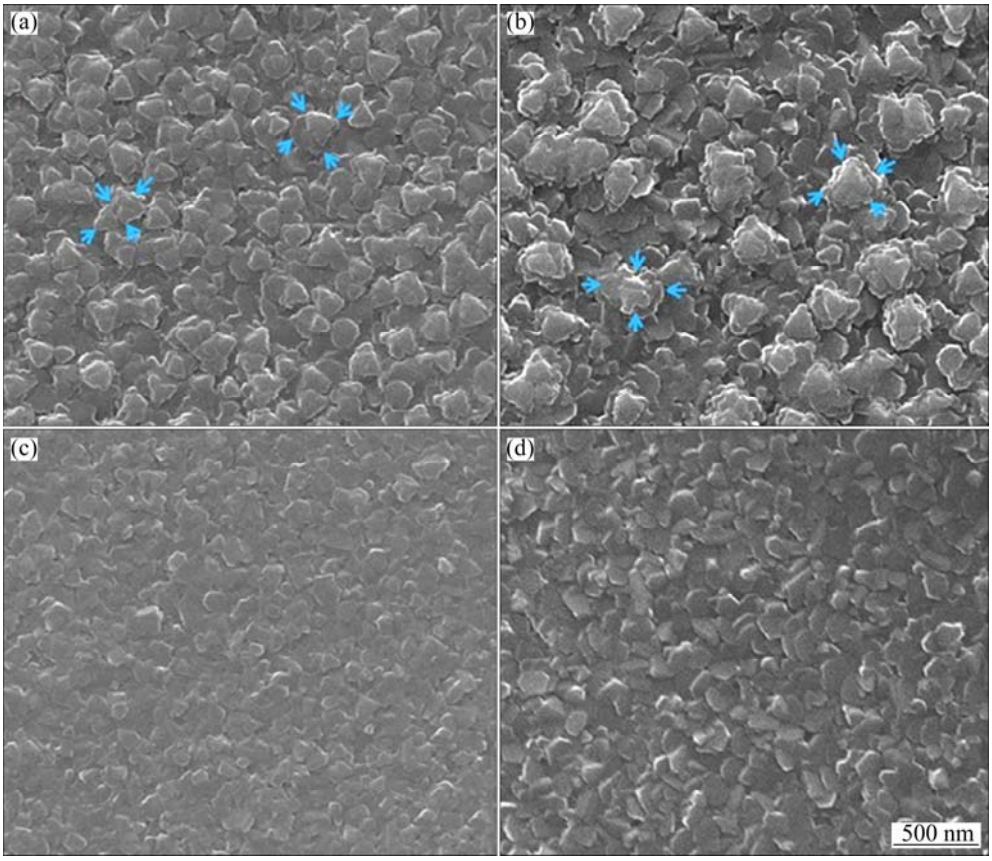

Fig. 2 SEM images of Ti films deposited at different bias voltages: (a) 0; (b) 60 V; (c) 100 V; (d) 140 V

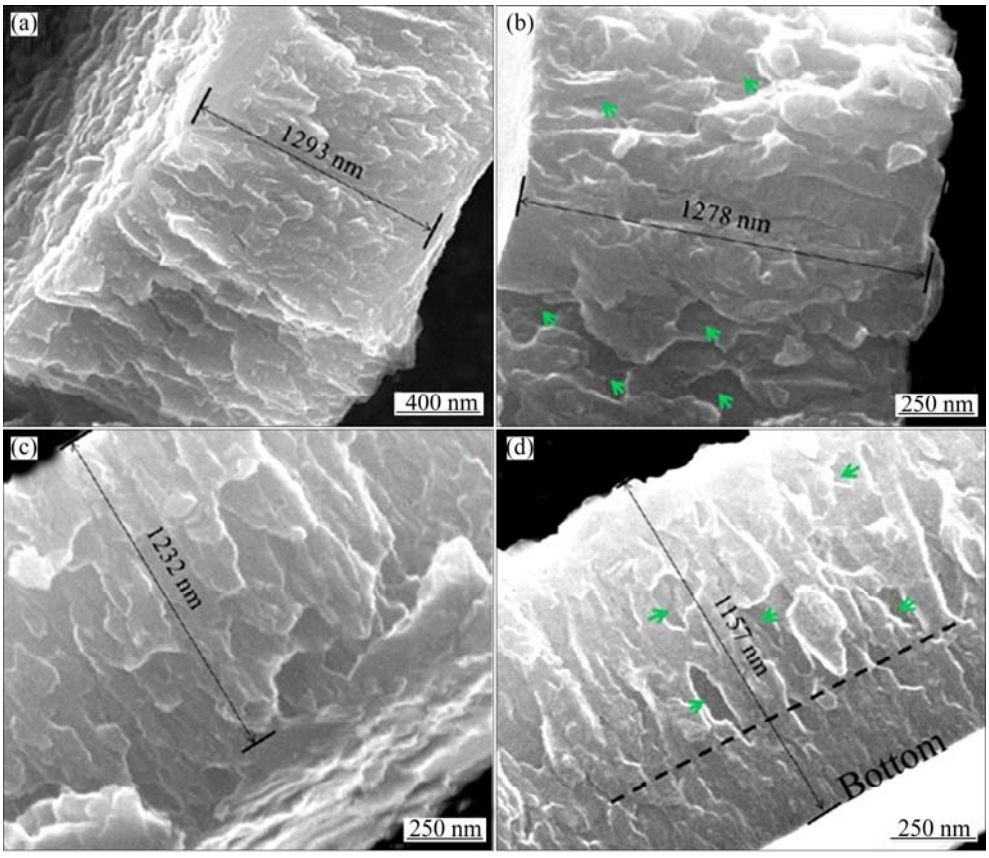

Fig. 3 Cross-sectional morphologies of Ti films deposited at different bias voltages: (a) 0; (b) 60 V; (c) 100 V; (d) 140 V

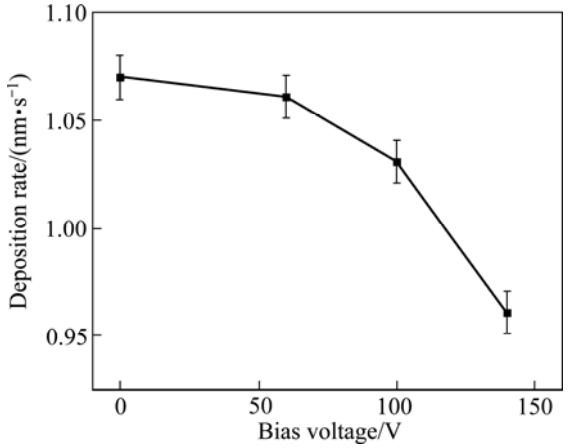

Fig. 4 Deposition rate of Ti films with dependence of bias voltage

3.3 Crystallinity

The typical TEM images of the Ti films sputtered at 0 and 100 V are shown in Fig. 5. The Ti film deposited at 0 V is composed of nanocrystallines (NC) and amorphous zones, as indicated by arrows in Fig. 5(a), respectively. The nanograins are separated by amorphous zones. Further evidence of the existence of amorphous zones is confirmed by the corresponding selected area electron diffraction (SAED) pattern, as shown in the inset of Fig. 5(a). The SAED pattern exhibits diffused and overlapped rings, suggesting a typical amorphous structure. The presence of an amorphous matrix is not detected using XRD, since the NC are well dispersed in the amorphous matrix (Fig. 5(a)). The amorphous-like topography of Ti film was observed by AFM, verified by JIN et al [16], and they attributed this amorphous-like structure to the low sputtering power of 100−150 W. JEYACHANDRAN et al [17] produced amorphous structure under the base pressure of 8×10^{-4}−13×10^{-4} MPa detected by XRD and they thought that the amorphous structure was related to the chemical composition of the pressure.

However, the crystallization is improved for the Ti film sputtered at 100 V, as shown in Fig. 5(b). The SAED (inset in Fig. 5(b)) also evidences the crystalline by the diffraction rings. The lattice spacing is 0.2325 nm corresponding to the (200) plane ($d_{(200)}$=0.2339 nm), as marked in Fig. 5(b). The (100) plane of Ti film is also observed ($d_{(100)}$=0.2574 nm), as shown in Fig. 5(b). These observations are in agreement with the XRD results. However, as indicated by arrows in Fig. 5(b), some amorphous zones still exist in the Ti film. The average grain size of Ti films estimated from TEM images ranges from 6 to 15 nm, and the smallest and largest grains are produced at the bias voltage of 0 and 100 V, respectively, as shown in Fig. 6.

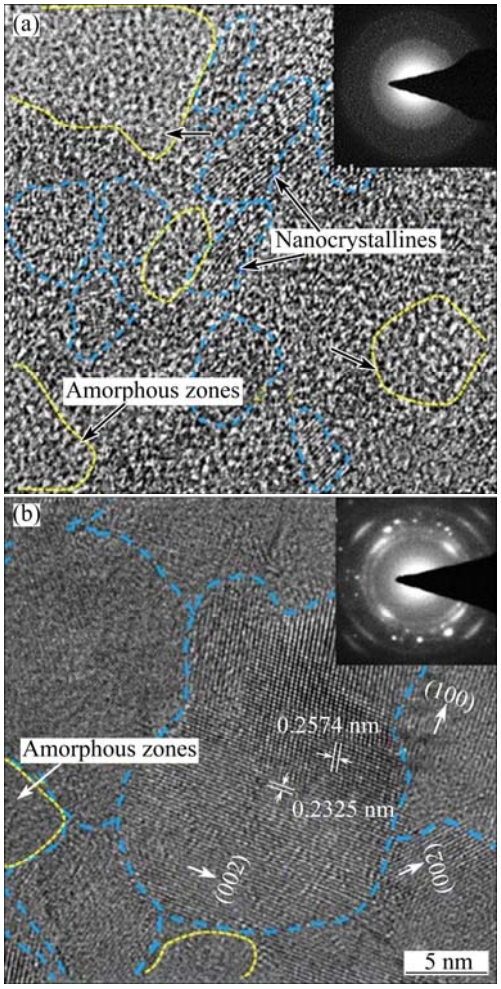

Fig. 5 Bright-field TEM images and corresponding selected area electron diffraction patterns of Ti films deposited at bias voltage of 0 (a) and 100 V (b)

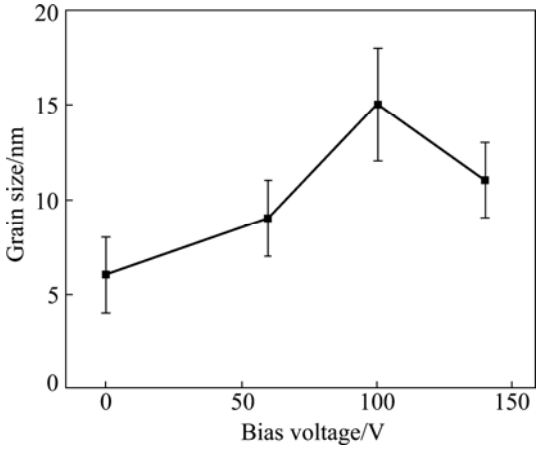

Fig. 6 Dependence of grain size on bias voltage

3.4 Hardness

The hardness was measured by indentation tests. In order to minimize the measurement error, two factors should be considered, e.g. the surface roughness and substrate effect. The surface roughness of Ti thin films

determined by AFM is 7−12 nm and the film thickness is 1157−1293 nm, as shown in Fig. 3. Thus, the indentation depth was controlled to be about 80 nm, within 7% of the film thickness. Figure 7(a) shows that the hardness (H) of Ti films firstly decreases from 4.75 GPa at 0 V to 3.91 GPa at 100 V and then increases slightly to 4.3 GPa at 140 V; The inset is the curves of nanoindentation tests. The smaller grain size should result in a higher hardness, deducted from the Hall−Petch (H−P) relationship ($H=H_0+Kd^{-1/2}$, where K is the H−P slope, and d is the average grain size). The H−P scaling law is shown in Fig. 7(b). The data of UFG Ti are originated from Ref. [18], where the UFG Ti plates with grain size of 168−453 nm were prepared by equal channel angular pressing. SERGUEEVA et al [19] also reported the hardness change of UFG Ti with grain size of 40−120 nm produced by high pressure torsion, and the experimental results are also shown in Fig. 7(b). Interesting, there apparently are two regions in the H−P rule, namely UFG and NC regions. However, the two zones show the different slopes of K, where the K_{UFG} is 0.61 MPa·m$^{1/2}$ and K_{NC} is 0.25 MPa·m$^{1/2}$ for the UFG and NC zones, respectively.

The H−P relationship is influenced by the microstructure, such as grain size [18−20], compressive stress, phase segregation [21], element substitution [22], compactness [23] and amorphous matrix [24]. For the pure metallic material, grain size is the main factor considered, and the other factors, such as dislocation, low-angle grain boundaries and twins, are generally not taken into account in evaluating H−P relationship. However, those structures exist extensively within UFG grains prepared by sever plastic deformation. This means that the K_{UFG} is likely to be overestimated. The higher K_{UFG} was observed in nanostructured Ni and Co by WANG et al [20]. They explained that the discrepancies could be due to the preexisting stacking faults and twins within nanograins or the different sample cutting methods. Owing to the difficulty of synthesizing truly NC Ti with d in the range of 0−100 nm, the H−P slope of Ti has not been extended into the very small d range. Although the slop, K, extends to the scale of 6−15 nm in the present work, two factors should be pointed out to influence the K_{NC}: 1) The orientation growth of the thin films might result in a higher hardness than randomly oriented film [25], thereafter, the higher K_{NC} should be expected; 2) It is not a true NC structure in the present work for the reason of amorphous structure existing in the nanocryatallines, hence, the hardness might also be enhanced by the amorphous structure resulting in a higher K_{NC}. The composite structure of nanocrystal grains and amorphous phase can increase the hardness, which was reported in the Ti−Si−N nanocomposite films [21,22,24]. For example, CHAWLA et al [24] thought that the improvement in the hardness of Ti−Si−N films was due to grain boundary hardening arising from the two phase structures of TiN nanocrystallites and Si_3N_4 amorphous matrix. From the two points above, the K_{NC} shall be lower than the present calculated value. In other words, the nanostructured Ti films might show a soft tendency characterized by a smaller K, which deviates the H−P relationship of the UFG zone. It should be noted that the H−P relationship of pure Ti requires further investigation by scaling the grain sizes in the range of 20−100 nm.

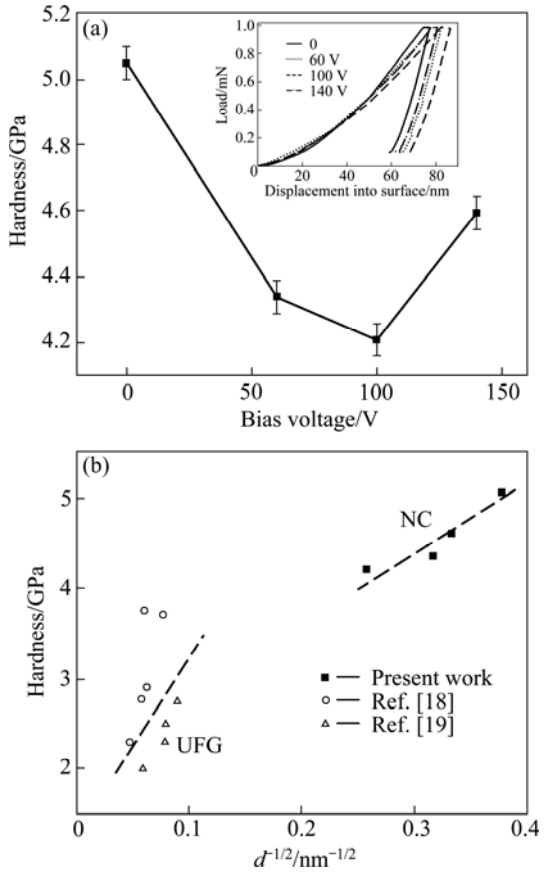

Fig. 7 Hardness changes with dependence of bias voltage (a) and grain size (b) (Inset in (a) is typical nanoindentation curves)

4 Discussion

The bias voltage mainly influences the crystallization, crystal orientation, grain size, and surface morphology of Ti films, as shown from XRD, SEM and TEM analysis. The bias voltage is related to the ion energy [26], expressed by $E \propto V_b/P^{1/2}$, where E, V_b and P are the ion energy, bias voltage and process pressure, respectively. The ion energy is proportional to V_b, which means that the kinetic energy of the ions increases with the bias voltage. An increasing kinetic energy makes the nucleation of a crystalline phase more easy [27], thereafter, the crystallization is improved compared with

the case without bias voltage. Since the (002) plane has the lowest surface free energy among all crystal planes introduced by CAI et al [28], the (002) preferred orientation is commonly produced during magnetron sputtering. However, grains with polycrystal orientation are formed with the increase of kinetic energy of the adatoms induced by the bias voltage, as shown in XRD patterns (Fig. 1) and TEM image (Fig. 5(b)). Thereafter, the (002) preferred orientation of Ti films is weakened with the increase of bias voltage. The other influence of bias voltage is the coarsening of grain size, which might be induced by the higher kinetic energy to activate the mobility of adatoms. As a result, the surface becomes denser and more homogeneous.

The magnetron sputtering has two processes: one is the deposition of adatoms and the other is secondary sputtering under the high kinetic energy. When the bias voltage is further increased to 140 V, the secondary sputtering effect of the adatoms becomes more obvious. The significant increase of kinetic energy leads to the departure of adatoms, which have already deposited on the Si substrate. The re-sputtering adatoms show a relative low kinetic energy compared with the firstly bombarded adatoms, therefore, (002) preferred orientation is enhanced again, as shown in XRD patterns (in Fig. 1). At the same time, the grain size and surface morphology are correspondingly changed. It is also because of the re-sputtering of adatoms, the deposition rate is decreased with increasing the bias voltage, and an accelerated decrease is observed at 140 V, as shown in Fig. 4.

5 Conclusions

1) A transition from (002) crystal orientation to polycrystal structure is observed with the increase of bias voltage within 100 V. While the bias voltage further increases to 140 V, and the (002) preferred orientation enhances again.

2) The grain size of Ti films is in the range of 6−15 nm, showing the maximum at the bias voltage of 100 V. The Ti films exhibit a composite structure of nanocrystallines and amorphous phase. Meanwhile, the crystallization is improved with the application of bias voltage.

3) The change of hardness is consistent with the grain size. The slop (K_{NC}) of Hall−Petch relationship is 0.25 MPa·m$^{1/2}$ in the scale of 6−15 nm.

References

[1] HSIEH S, BECK D, MATSUMOTO T. Thermal stability of ultrathin titanium films on a Pt (111) substrate [J]. Thin Solid Films, 2004, 466: 123−127.

[2] PADHY N, MUDALI U K, CHAWLA V. Corrosion behaviour of single (Ti) and duplex (Ti−TiO_2) coating on 304L stainless steel in nitric acid medium [J]. Mater Chem Phys, 2011, 130: 962−972.

[3] CHU C L, HU T, WU S L, WANG R M, DONG Y S, LIN P H, CHUNG C Y, CHU P K. In situ synthesis of nanostructured titania film on NiTi shape memory alloy by Fenton's oxidation method [J]. Transactions of Nonferrous Metals Society of China, 2007, 17: 902−906.

[4] CHAWLA V, JAYAGANTHAN R, CHAWLA A K. Microstructural characterizations of magnetron sputtered Ti films on glass substrate [J]. J Mater Process Techn, 2009, 209: 3444−3451.

[5] ZHOU W, LIU C, SUN Q, ZHANG K, MU H W. Research on optical reflective properties of $Ni_{56}Mn_{27}Ga_{17}$ alloy thin films fabricated by magnetron sputtering [J]. Optical Instruments, 2013, 3: 77−79. (in Chinese)

[6] ZHANG L, SHI L Q, HE Z J. Deposition of dense and smooth Ti films using ECR plasma-assisted magnetron sputtering [J]. Surf Coat Technol, 2009, 203: 3356−3360.

[7] YAN H, ZHAO F. Advances in reactive magnetron sputtering (RMS) applied on optical coating [J]. Optical Instruments, 2004, 2: 109−114. (in Chinese)

[8] CHAWLA V, JAYAGANTHAN R, CHAAWL A K. Morphological study of magnetron sputtered Ti thin films on silicon substrate [J]. Mater Chem Phys, 2008, 111: 414−418.

[9] LAN D, LAI Q, HUANG S H, ZOU M. Effects of sputtering parametres on the structure of Ti film on the Ni-free 201 stainless steel and evaluation of film adhesiveness to the base [J]. Rare Metal Mat Eng, 2011, 40(S2): 409−412. (in Chinese)

[10] SHUANG H H, QI L. The deposition rate of Ti film by plasma [J]. Mechatronics Mater Process I, 2011, 328−330: 1120−1123.

[11] QI L, SHUANG H H. The effect of preparation conditions to crystal of Ti film [J]. Mechatronics Mater Process I, 2011, 328−330: 1339−1342.

[12] ZHANG L L, DENG A H, YANG D X. Bias effects on the growth of helium-containing titanium films [J]. Chin Phys Lett, 2011, 28: 077802.

[13] QI L, SHUANG H H, DE J L. Effects of negative bias on the structure of Ti film and its adhesiveness to the base by plasma [J]. Mech Aerospace Eng, 2011, 110−116: 592−595.

[14] VELA M, CACERES D, PRIETO C. Mechanical properties of sputtered silicon nitride thin films [J]. J Appl Phys, 2003, 94: 7868−7873.

[15] ZHANG X Q, KE P L, WANG A Y, HUANG M D, KIM K H. Effect of substrate bias on microstructure and tribological performance of GLC films using hybrid HIPIMS technique [J]. Transactions of Nonferrous Metals Society of China, 2012, 22(S3): s740−s744.

[16] JIN Y Z, WU W, LI L. Effect of sputtering power on surface topography of dc magnetron sputtered Ti thin films observed by AFM [J]. Appl Surf Sci, 2009, 255: 4673−4679.

[17] JEYACHANDRAN Y L, KARUNAGARAN B, NARAYANDASS S K. Properties of titanium thin films deposited by dc magnetron sputtering [J]. Mater Sci Eng A, 2006, 431: 277−284.

[18] LI Y K, LIU F, ZHENG G P. Strength scaling law, deformation kinetics and mechanisms of nanostructured Ti [J]. Mater Sci Eng A, 2013, 573: 141−147.

[19] SERGUEEVA A V, STOLYAROV V V, VALIEV R Z. Advanced mechanical properties of pure titanium with ultrafine grained structure [J]. Scripta Mater, 2001, 45: 747−752.

[20] WANG Y M, OTT R T, BUUREN T V. Controlling factors in tensile deformation of nanocrystalline cobalt and nickel [J]. Phys Rev B, 2012, 85: 014101.

[21] ZHANG Y J, YANG Y Z, ZHAI Y H, ZHANG P Y. Effect of negative substrate bias on the microstructure and mechanical properties of Ti−Si−N films deposited by a hybrid filtered cathodic arc and ion beam sputtering technique [J]. Appl Surf Sci, 2012, 258:

6897−6901.
[22] ZHANG P, CAI Z H, XIONG W Q. Influence of Si content and growth condition on the microstructure and mechanical properties of Ti−Si−N nanocomposite films [J]. Surf Coat Technol, 2007, 201: 6819−6823.
[23] CHOIA S R, PARKA I W, KIMB S H, KIM K H. Effects of bias voltage and temperature on mechanical properties of Ti–Si–N coatings deposited by a hybrid system of arc ion plating and sputtering techniques [J]. Thin Solid Films, 2004, 447−448: 371−376.
[24] CHAWLA V, JAYAGANTHAN R, CHANDRA R. A study of structural and mechanical properties of sputter deposited nanocomposite Ti−Si−N thin films [J]. Surf Coat Technol, 2010, 204: 1582−1589.
[25] TANG X F, LUO F, OU F. Effects of negative substrate bias voltage on the structure and properties of aluminum oxide films prepared by DC reactive magnetron sputtering [J]. Appl Surf Sci, 2012, 259: 448−453.
[26] WANG Y X, WANG L P, ZHANG G G. Effect of bias voltage on microstructure and properties of Ti-doped graphite-like carbon films synthesized by magnetron sputtering [J]. Surf Coat Technol, 2010, 205: 793−800.
[27] SRIDHARAN M, SILLASSEN M, BOTTIGER J. Pulsed DC magnetron sputtered Al_2O_3 films and their hardness [J]. Surf Coat Technol, 2007, 202: 920−924.
[28] CAI K, MULLER M, BOSSERT J. Surface structure and composition of flat titanium thin films as a function of film thickness and evaporation rate [J]. Appl Surf Sci, 2005, 250: 252−267.

偏压对钛薄膜显微组织及力学性能的影响

刘颍龙[1]，刘 芳[2]，吴 倩[2]，陈爱英[2]，李 翔[2]，潘 登[2]

1. 上海理工大学 机械工程学院，上海 200093；
2. 上海理工大学 材料科学与工程学院，上海 200093

摘 要：为了研究纳米结构金属 Ti 的纳米力学性能，在偏压为 0~140 V 的范围内，采用磁控溅射方法制备纯钛薄膜。并采用 X 射线衍射仪(XRD)、扫描电子显微镜(SEM)和高分辨率透射电子显微镜(HRTEM)表征钛薄膜的显微组织。结果表明：钛薄膜呈现非晶与纳米晶的混合结构，且晶化程度随着偏压的升高而增大。纳米压痕测试结果表明：钛薄膜的硬度与晶粒尺寸在 6~15 nm 的范围内符合 Hall−Petch 关系。但其 Hall−Petch 关系的斜率与采用其他强烈塑性变形法制备的超细晶纯钛相比，明显偏小，且呈现软化趋势。此外，讨论偏压对钛薄膜生长取向的影响。

关键词：钛薄膜；磁控溅射；偏压；纳米晶；Hall−Petch 关系

(Edited by Chao WANG)